Heterogeneous silver–polyaniline nanocomposites with tunable morphology and controllable catalytic properties

2013 Nanotechnology 24 185602

(http://iopscience.iop.org/0957-4484/24/18/185602)

Nanotechnology **24** (2013) 185602 (9pp) doi:10.1088/0957-4484/24/18/185602

Heterogeneous silver–polyaniline nanocomposites with tunable morphology and controllable catalytic properties

Conghui Yuan[1,2], Yiting Xu[2], Lina Zhong[2], Long Zhang[2], Cangjie Yang[2], Binjie Jiang[2], Yuanming Deng[2], Birong Zeng[2], Ning He[1], Weiang Luo[2] and Lizong Dai[2]

[1] College of Chemistry and Chemical Engineering, Xiamen University, Xiamen, 361005, People's Republic of China
[2] Fujian Provincial Key Laboratory of Fire Retardant Materials, College of Materials, Xiamen University, Xiamen, 361005, People's Republic of China

E-mail: henig@xmu.edu.cn and lzdai@xmu.edu.cn

Received 9 January 2013, in final form 15 March 2013
Published 10 April 2013
Online at stacks.iop.org/Nano/24/185602

Abstract
This paper introduces not only a simple hydrothermal route to silver–polyaniline (Ag–PANI) nanocomposites with controllable morphology, but also a type of catalyst possessing tunable and switchable catalytic capability. Ag–PANI Janus nanoparticles (NPs) and Ag@PANI core–shell NPs have been constructed successfully at different hydrothermal temperatures. The diameter of both Ag and PANI hemispheres of Janus NPs, as well as the PANI shell thickness of core–shell NPs, was finely tuned via adjustment of the feed ratio. We also gained a deeper insight into the functionalities of PANI components in the catalytic capability of the heterogeneous catalysts, choosing catalytic reductions of nitrobenzene (NB) and 4-nitrophenol (4-NP) as model reactions. Our results showed that the catalytic capability of the nanocomposites was dependent on the PANI morphology and hydrophobicity. The PANI shell coating on Ag NPs can concentrate the lipophilic NB, thus leading to an enhanced catalytic capability of Ag@PANI core–shell NPs. However, this enhanced catalytic capability was not observed for Ag–PANI Janus NPs when catalytically reducing NB. More importantly, the catalytic capability of the core–shell NPs in the reduction of hydrophilic 4-NP is switchable by varying the PANI shell from an undoped to a doped state.

S Online supplementary data available from stacks.iop.org/Nano/24/185602/mmedia

(Some figures may appear in colour only in the online journal)

1. Introduction

Breaking the geometrical symmetry and the component uniformity always renders nanoparticles (NPs) a unique architectur with a multifunctionality that has profound applications in nanodevices and nanoreactors. This has promising implications, but is also a challenge in materials science and engineering. Janus NPs, named after the two-faced Roman god and possessing two incompatible sides, are a typically advanced material with anisotropic geometry. By combining two hemispheres with different components or chemical properties, inorganic [1–3], organic–inorganic [4–6] and polymeric [7–9] Janus NPs have been constructed via some universal routes such as toposelective surface modification [10–15], molecular self-assembly [8, 9] and microfluidic methods [16, 17]. Core–shell structure NPs, especially those with one core in each capsule, represent another important direction of heterogeneous nanomaterials. The significance of this structure is derived from the component difference between the core and shell, which endows the core–shell NPs with tunable physicochemical properties. Over the past decades, many noble metal

NPs have been encapsulated in functional polymer shells successfully through self-assembly or surface polymerization methods [18–24]. Polymer shells can protect and stabilize the encapsulated noble metal NPs. However, they also allow matter and energy exchange between the interior and exterior shell environments, therefore resulting in promising applications in optical [20–23] and catalytic fields [25–29].

Here we report a facile hydrothermal route to heterogeneous silver–polyaniline (Ag–PANI) Janus NPs and Ag@PANI core–shell NPs. Normally, the direct reaction between aniline (ANI) and Ag^+ is too fast and uncontrollable. As a result, the obtained Ag–PANI composite materials show random and unpredictable morphologies [30, 31]. Inspired by the low oxidation potential of insoluble silver composite, we speculate that the silver dodecyl benzene sulfonate (DBS–Ag) may possess a controllable reducing speed under hydrothermal conditions by using aniline (ANI) as reducing agent. DBS–Ag is readily obtained from the reaction between $AgNO_3$ and sodium dodecyl benzene sulfonate (SDBS). Indeed, hybrid nanocomposites with core–shell and Janus structures have been prepared at different hydrothermal temperatures. We also envisioned that the PANI component would regulate the catalytic capability of the hybrid nanocomposites. The catalytic reductions of nitrobenzene (NB) and 4-nitrophenol (4-NP) were chosen as model reactions to comparatively evaluate the catalytic properties of core–shell NPs and Janus NPs. PANI shells can regulate the mass transfer during the catalytic reduction of NB and 4-NP, including concentrating the reagent and switching the penetration of reactants. Conversely, no significant functionality was observed for the PANI component in Janus NPs during the reduction of NB. We demonstrate in this work not only the controllable morphology of the hybrid nanocomposite, but also the mechanism by which the PANI component regulates the catalytic properties of the hybrid catalysts.

2. Experimental details

Chemicals. $AgNO_3$ and SDBS were purchased from Alfa Aesar. ANI was supplied by Aldrich and redistilled before use. NB, 4-NP, *N*-methyl pyrrolidone and sodium borohydride ($NaBH_4$) were obtained from Shanghai Chemical Reagent Industry.

Synthesis of Ag–PANI Janus NPs. 0.4 g (1.2 mmol) of SDBS and 0.2 ml (2.2 mmol) of ANI were dissolved in 40 ml of deionized water to form 30.0 and 55.0 mmol l^{-1} concentrations, respectively. The mixture was stirred for 30 min at 40 °C to obtain a clear solution. 0.085 g (0.1 mmol) of $AgNO_3$ was added into the mixture. After stirring for 30 min at room temperature, the reaction solution turned milky. The mixture was poured into a hydrothermal reactor and left undisturbed in an oven at a temperature of 105 °C for 12 h. After cooling down to room temperature, Ag–PANI Janus NPs were prepared. To purify the product, the mixture was centrifuged at 3500 rad min^{-1} and washed with water three times. We also used 27.5, 110.0 and 165.0 mmol l^{-1} of ANI to examine the influence of the concentration of ANI on the morphology of the resultant product. Ag–PANI Janus NPs prepared from 27.5, 55, 110.0 and 165.0 mmol l^{-1} of ANI were marked as Janus **1**, Janus **2**, Janus **3** and Janus **4**, respectively.

Synthesis of Ag@PANI core–shell NPs. The only difference between the syntheses of Ag@PANI core–shell NPs and Ag–PANI Janus NPs is the hydrothermal temperature. Simply, 0.4 g (1.2 mmol) of SDBS and 0.2 ml (2.2 mmol) of ANI were dissolved in 40 ml of deionized water at 40 °C to obtain 30.0 and 55.0 mmol l^{-1} concentrations, respectively. After the addition of 0.085 g (0.1 mmol) $AgNO_3$ into the solution at room temperature, the mixture turned milky immediately. The mixture was poured into a hydrothermal reactor and left undisturbed in an oven at a temperature of 125 °C for 12 h. Then, the mixture containing the product was cooled down to room temperature and centrifuged at 3500 rad min^{-1}. After drying at 60 °C for 24 h, the Ag@PANI core–shell NPs were obtained. To control the thickness of the PANI shell, different concentrations of ANI such as 27.5, 110.0, 165.0 and 220.0 mmol l^{-1} were used. We marked the Ag@PANI core–shell NPs prepared from 27.5, 55.0, 110.0, 165.0 and 220.0 mmol l^{-1} of ANI as core–shell **1**, core–shell **2**, core–shell **3**, core–shell **4** and core–shell **5**, respectively.

Synthesis of Ag NPs. 0.4 g (1.2 mmol) of SDBS and 0.085 g (0.1 mmol) of $AgNO_3$ were dissolved in 40 ml of deionized water and the mixture was stirred for 30 min at 40 °C to obtain a milky solution. After the addition of 0.038 g of (1.0 mmol) $NaBH_4$, the mixture was left undisturbed at room temperature for 4 h. The mixture containing the key product was dialyzed in water using a dialytic-bag (molecular weight cutoff 3500) to remove unreacted materials and byproducts. Pure Ag NPs were obtained by centrifuging the mixture at 3500 rad min^{-1}.

Catalytic reduction of NB and 4-NP. In the case of NB, an aqueous solution of NB (0.04 ml, 0.01 M) was added into a quartz cuvette filled with 2.0 ml deionized water under magnetic stirring. $NaBH_4$ aqueous solution (0.4 ml, 0.1 M) together with the Ag@PANI NP, Ag–PANI Janus NP or Ag NP (0.1 ml, 0.05 mg ml^{-1}) aqueous solutions were added to the quartz cuvette. UV/vis spectra were recorded at regular time intervals to monitor the progress of the reaction.

In the case of 4-NP, two feeding sequences were applied. First, 4-NP, $NaBH_4$ and Ag@PANI NP (or Ag NP) aqueous solutions were added into a quartz cuvette filled with 2.0 ml deionized water synchronously. Second, 4-NP and Ag@PANI NPs aqueous solutions were firstly added into a quartz cuvette filled with 2.0 ml deionized water. The mixture was left undisturbed at room temperature for 0.5 h, and then $NaBH_4$ aqueous solution was added. All the concentrations of the chemicals used here were the same as those in the case of NB. UV/vis spectra were also recorded at regular time intervals to monitor the reaction.

For all these measurements, the oxygen in 2.0 ml of deionized water was first removed by purging it with a flow of argon for 30 min before the reducing reaction. All experiments were carried out at least three times to check the reproducibility.

Characterization. Transmission electron microscope (TEM) measurements and electron diffraction experiments were

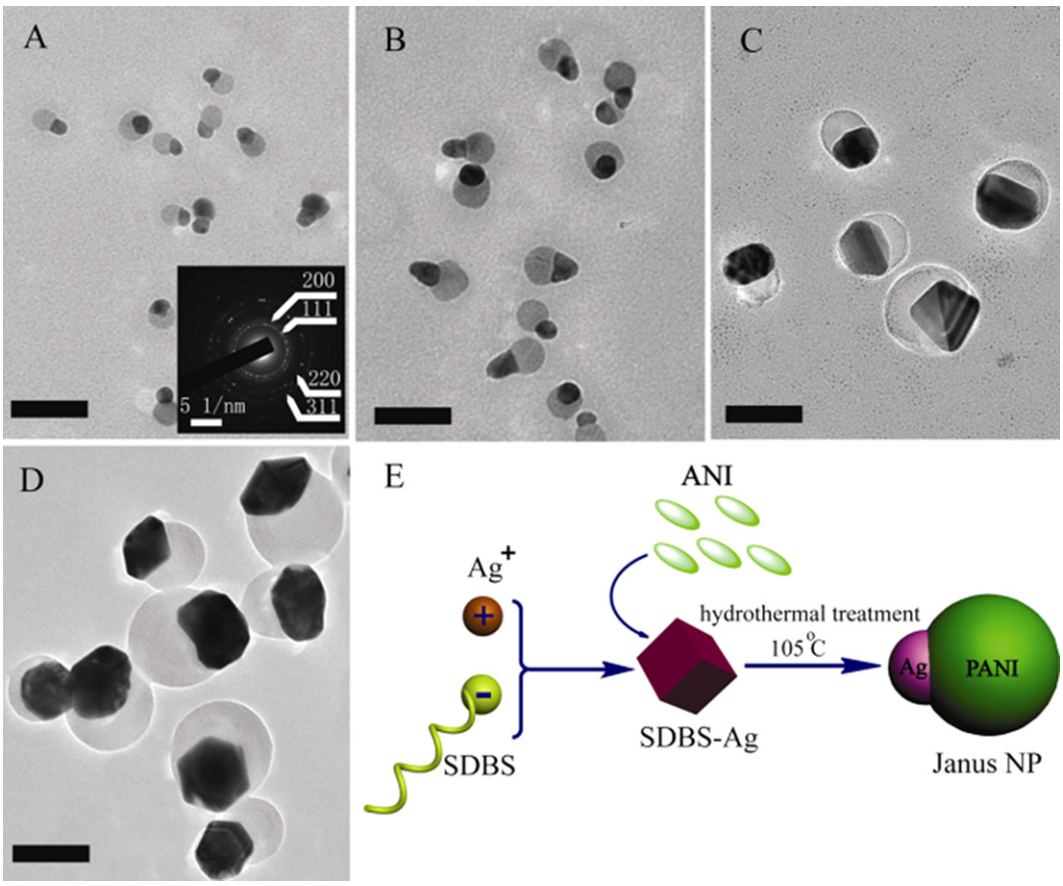

Figure 1. TEM images of Ag–PANI Janus NPs prepared using (A) 27.5, (B) 55.0, (C) 110.0 and (D) 165.0 mmol l^{-1} of ANI, all scale bars in TEM images are 100 nm. Inset of (A) is the electron diffraction pattern of Ag–PANI Janus NPs. (E) Schematically illustrates the formation process of the Ag–PANI Janus NPs.

performed with a JEM2100 microscope at an acceleration voltage of 200 kV. The crystallization behaviors of the samples were investigated by using an x-ray diffraction (XRD) diffractometer (Panalytical X'Pert diffractometer with Cu Kα_1 radiation, 40 keV, 30 mA). UV/vis spectra of the samples in aqueous solutions were measured on a Unico UV/vis 2802PCS instrument. The content of the Ag component in the Ag–PANI nanocomposite was tested by thermogravimetric analyzer (TGA) on a Netzsch STA 409EP. The dry samples were heated to 800 °C under 30 ml min^{-1} nitrogen with a heating rate of 10 °C min^{-1} (see figure 1S for the results available at stacks.iop.org/Nano/24/185602/mmedia). Dynamic light scattering (DLS) measurements were performed using a Malvern Nanozetasizer. The surface area of Ag NPs was calculated under the hypothesis that all Ag NPs are spherical. The average diameter of the Ag NPs was statistically calculated from every 100 nanostructures in TEM images, and the bulk density of Ag used here was 10.53 g cm^{-3}.

3. Results and discussion

3.1. Structure

In the reaction system, surfactant SDBS acts as a soft template, as well as a reaction material interacting with Ag^+ to form insoluble salt DBS–Ag. The reduction of DBS–Ag by ANI under hydrothermal treatment leads to the formation of Ag NPs at a controllable rate. Synchronously, the oxidation of ANI results in the formation of the PANI component which conjugates with the Ag NPs to form Janus or core–shell structures. We first tested the possibility of morphology control. Three hydrothermal temperatures—105, 125 and 115 °C—were applied during the preparation of the hybrid composites.

Ag–PANI hybrid composites obtained at hydrothermal temperature of 105 °C show a clear Janus structure (figures 1(A)–(D)). Each Ag–PANI Janus NP is composed of an Ag hemisphere and a PANI hemisphere. The size control of both Ag and ANI hemispheres was achieved by varying the concentration of AIN at a constant $AgNO_3$ concentration. Janus **1**–**4**, representing Ag–PANI Janus NPs prepared using 27.5, 55.0 110.0 and 165.0 mmol l^{-1} of ANI, exhibited average diameters (statistically calculated from 100 nanostructures in TEM images) of Ag hemispheres ranging from 15 to 80 nm, whereas the average diameters of PANI hemispheres ranged from 30 to 110 nm. The trend over particle size was also confirmed by the DLS measurements (figure 2S available at stacks.iop.org/Nano/24/185602/mmedia). The inset of figure 1(A) displays the electron diffraction pattern of the Ag–PANI Janus NPs. Clear diffraction disks represent the {111}, {200}, {220} and {311}

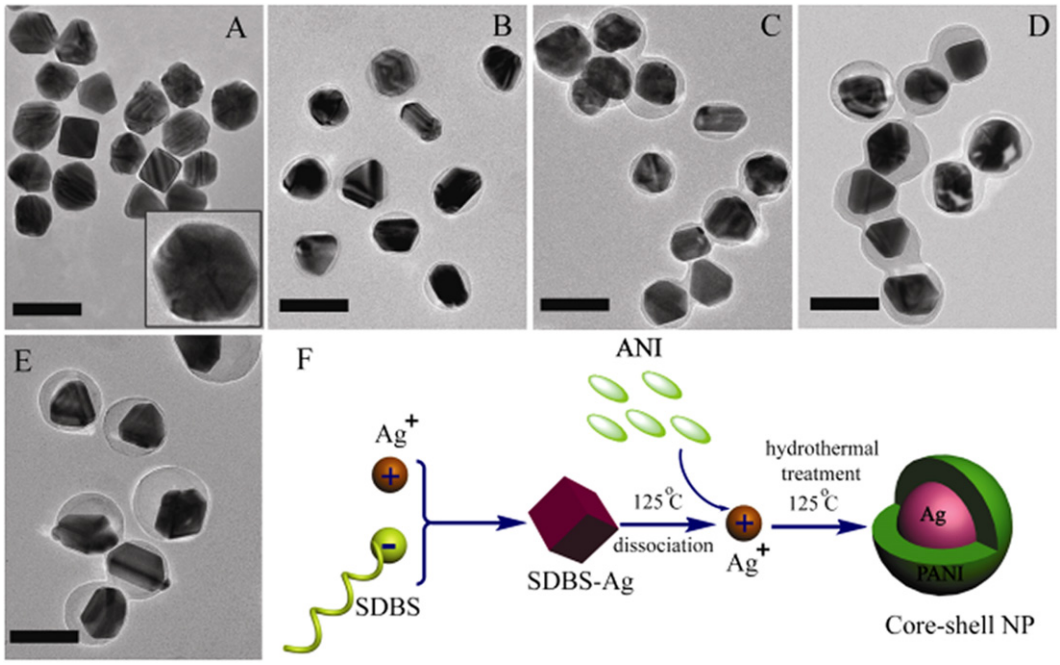

Figure 2. TEM images of Ag@PANI core–shell NPs prepared using (A) 27.5, (B) 55.0, (C) 11.0, (D) 165.0 and (E) 220.0 mmol l^{-1} of ANI, all scale bars are 100 nm. The inset of (A) is the magnified TEM image of Ag@PANI core–shell NPs. (F) Schematically simulates the formation process of Ag@PANI core–shell NPs.

Ag crystal planes, which accord well with the results shown in the XRD patterns (figure 3S available at stacks.iop.org/Nano/24/185602/mmedia). The evident absorption peak at 360 nm in the UV/vis spectra of Ag–PANI Janus NPs (figure 4S) reveals the presence of the PANI component. Moreover, a gradual red-shift (from 415 to 480 nm) of the absorption peak attributed to Ag NPs was observed in the UV/vis spectra, which also indicates the diameter increase of Ag hemispheres.

We proposed a mechanism for the formation of the Janus morphology (figure 1(E)). Since the insoluble salt DBS–Ag has a small dissociation constant, the concentration of Ag^+ in solution would be extremely low. As a result, it is difficult for the ANI to reduce the dissociated Ag^+. However, the reduction of Ag^+ on the surface of DBS–Ag crystals is possible (the appearance of milky solution when mixing SDBS with $AgNO_3$ in deionized water and figure 5S (available at stacks.iop.org/Nano/24/185602/mmedia) support the formation of DBS–Ag crystals). This is due to the dissociation equilibrium between DBS–Ag and Ag^+, which makes the concentration of Ag^+ on the DBS–Ag surface much higher than that in bulk solution. After the formation of the Ag core on the DBS–Ag surface, only part of the Ag surface is exposed to the aqueous solution. In this case, aniline can be only polymerized on the exposed Ag surface, because aniline cannot diffuse through the DBS–Ag component. As a result, Ag and PANI hemispheres grow up along opposite directions, thus constructing the Janus structure. Briefly, we speculate that the reduction of Ag^+ on the surface of DBS–Ag NPs is the key factor leading to the formation of Ag–PANI Janus NPs.

Next, we increased the hydrothermal temperature to 125 °C. Notably, all resultant products exhibit a well-defined core–shell structure (figure 2). Since the PANI shell of the Ag@PANI NPs (referred as core–shell **1**) obtained from 27.5 mmol l^{-1} ANI is too thin to visualize (figure 2(A)), a magnified TEM image of this core–shell NPs is shown in the inset of figure 2(A). The average thickness of the PANI shell was calculated to be 2 ± 0.4 nm. With increasing ANI concentration, the thickness of the PANI shell increased clearly. Core–shell **2**–**5** representing the Ag@PANI NPs obtained by using 55.0, 110.0, 165.0 and 220.0 mmol l^{-1} of ANI possessed average shell thicknesses of about 5 ± 1.0, 11 ± 3.0, 22 ± 5.0 and 29 ± 7.0 nm, respectively (statistically analyzed from 100 nanostructures in TEM images, figures 2(B)–(E)). This trend over shell thickness was also observed in the DLS results (figure 2S available at stacks.iop.org/Nano/24/185602/mmedia). These results suggest that the average thickness of the PANI shell could be controlled by simply adjusting the concentration of ANI. An electron diffraction pattern (figure 6S available at stacks.iop.org/Nano/24/185602/mmedia) of the Ag@PANI NPs indicates that Ag NPs encapsulated in PANI shells have a similar crystal form to that in Ag–PANI Janus NPs. The UV/vis spectra also suggest that the shells of core–shell NPs are composed of PANI (figure 7S available at stacks.iop.org/Nano/24/185602/mmedia).

We suggested another mechanism for the growth of the core–shell structure at a hydrothermal temperature of 125 °C (figure 2(F)). Note that the dissociation constant of the insoluble salt normally increases with increasing temperature. We assume that the concentration of the dissociated Ag^+ at 125 °C is much higher than that at 105 °C. Accordingly, it is possible for ANI to reduce Ag^+ in aqueous solution. This means that the Ag nanocrystal cores form in aqueous solution, rather than on the surface of DBS–Ag NPs. Then,

Table 1. Catalytic capability for the reduction of NB and some relative parameters of the Ag–PANI Janus NPs, Ag@PANI core–shell NPs and Ag NPs. (Note: K_{app}: apparent rate constant; K_1: rate constant normalized to the surface of the Ag NPs in solution (see equation (1)); W: content of Ag in the Ag–PANI nanocomposites; C: actual concentration of the Ag component in solution; d: average diameter of the Ag NPs; S: actual surface area of Ag NPs normalized to the unit volume of the solution. K_{app} and K_1 were calculated under three assumptions: (1) Ag NPs are spherical; (2) low conversions.)

Samples	K_{app} (s^{-1})	K_1 (s^{-1} m^{-2} l)	W (wt%)	C (mg ml^{-1})	d (nm)	S (m^2 l^{-1})
Janus **3**	1.21×10^{-3}	6.84×10^{-2}	75.9	1.88×10^{-3}	61.1 ± 9	1.77×10^{-2}
Core–shell **1**	1.38×10^{-3}	6.16×10^{-2}	97.8	2.45×10^{-3}	63.5 ± 6	2.24×10^{-2}
Core–shell **2**	1.43×10^{-3}	6.74×10^{-2}	92.2	2.31×10^{-3}	62.2 ± 6	2.12×10^{-2}
Core–shell **3**	1.88×10^{-3}	9.94×10^{-2}	85.5	2.14×10^{-3}	64.6 ± 8	1.89×10^{-2}
Core–shell **4**	3.30×10^{-3}	1.92×10^{-1}	74.8	1.87×10^{-3}	62.1 ± 4	1.72×10^{-2}
Core–shell **5**	3.41×10^{-3}	2.42×10^{-1}	64.4	1.61×10^{-3}	65.2 ± 8	1.41×10^{-2}
Ag NPs	1.76×10^{-3}	8.68×10^{-2}	100	2.50×10^{-3}	63.2 ± 5	2.31×10^{-2}

the oxidation of ANI on the Ag core finally results in the construction of the core–shell nanostructure. Since the reducing reaction rates in every direction are not always the same, it is reasonable to assume that Ag cores shown in figures 2(A)–(E) are not located at the center of the Ag@PANI NPs. We have also tried to use 115 °C as the hydrothermal temperature to prepare Ag–PANI hybrid composite. The TEM result (shown in figure 8S available at stacks.iop.org/Nano/24/185602/mmedia) indicates that the resultant product contains both Janus and core–shell structures. This implies that the hydrothermal temperature is the key factor that determines the morphology of the Ag–PANI nanocomposite.

We also noted that there is no change in the diameter of Ag cores shown in figure 2. This is significantly different from the trend of Ag NPs in Janus NPs. We speculate that this is induced by the higher hydrothermal temperature. Ag cores form and grow up immediately at 125 °C, making the quantity of the Ag cores in the system constant throughout the reaction. Consequently, after the polymerization of ANI, a low concentration of ANI results in a thin PANI shell, whereas a high concentration of ANI leads to a thick PANI shell. To this end, it is reasonable to consider that this hydrothermal method demonstrates a simple and efficient route to Ag–PANI nanocomposites with controllable morphology.

3.2. Tunable catalytic capability

Nanosized polymer structures have been demonstrated to be attractive in catalyst system, since they can provide ideal scaffolds for supporting the catalyst, as well as creating a favorable nanoenvironment to concentrate the reagent phase [32–34]. This is especially useful in the catalytic reaction of hydrophobic regents in a water solution. The hydrophobic or amphiphilic polymer scaffold can act as a bridge to combine the catalyst with the reagent [35]. Encapsulation of nanocatalyst using a polymer shell is also a typical route to tune the catalytic capability. For example, a thermally sensitive poly(*N*-isopropylacrylamide) shell renders the encapsulated Ag core a temperature-dependent catalytic capability in the reduction of NB [25]. Similarly, we have also demonstrated in previous work that the mesoporous polystyrene shell coating on the Au NP permits only the entrance of hydrophobic NB [36].

Here, we are interested in demonstrating that the access of small molecules into the hybrid nanocomposite catalyst can be controlled by: (i) variation in the PANI morphology; (ii) adjustment of the PANI size; and (iii) change of the PANI property (undoped/doped state).

First, Janus **3** and core–shell **4** were adopted to test the effect of PANI morphology on the catalytic capability, when catalytically reducing NB to ANI by using $NaBH_4$. The reason for this choice is that these two nanocomposites possess similar Ag NP size (~60 nm) and PANI weight percentage (~25%), which makes the comparison justifiable and accurate. The catalytic reaction of NB was traced UV/vis spectra. A significant decrease in the absorption peak of NB (267 nm) and increase in the absorption peak of ANI (232 nm) suggests that both Janus and core–shell NPs can catalyze the reduction of NB into ANI (figures 3(A) and (B)). Interestingly, we observed an evident difference in the trend between these two catalytic reactions. The reaction catalyzed by Janus NPs occurred immediately upon mixing of all reagents, whereas the reaction catalyzed by core–shell NPs exhibited a long induction period (around 30.0 min, figure 3(C)). However, if disregarding the induction period, the reaction kinetics (analyzed according to equation (1)) of the two reactions at a relatively low conversion reveal that the core–shell NPs have a higher catalytic capability (figure 3(D)). The K_{app} (apparent rate constant) and K_1 (rate constant normalized to the surface of the Ag NPs) of the reaction catalyzed by core–shell NPs are calculated to be 3.30×10^{-3} s^{-1} and 1.92×10^{-1} s^{-1} m^{-2} l (table 1). These parameters are larger than that of the reaction catalyzed by Janus NPs.

$$-\frac{dc_t}{dt} = K_{app}c_t = K_1 S c_t. \quad (1)$$

Here K_{app} represents the apparent rate constant, c_t is the concentration of NB at time t and K_1 is the rate constant normalized to S, the surface area of Ag NPs normalized to the unit volume of the reaction system. Because $NaBH_4$ was used in a large excess, the concentration of $NaBH_4$ is disregarded in this equation [26].

Next, we chose Ag@PANI core–shell NPs with different shell thicknesses to test the possibility of catalytic capability control by varying the PANI size. The advantage of using these core–shell NPs is that all the Ag@PANI core–shell NPs exhibit the similar Ag diameter (~60 nm). It was

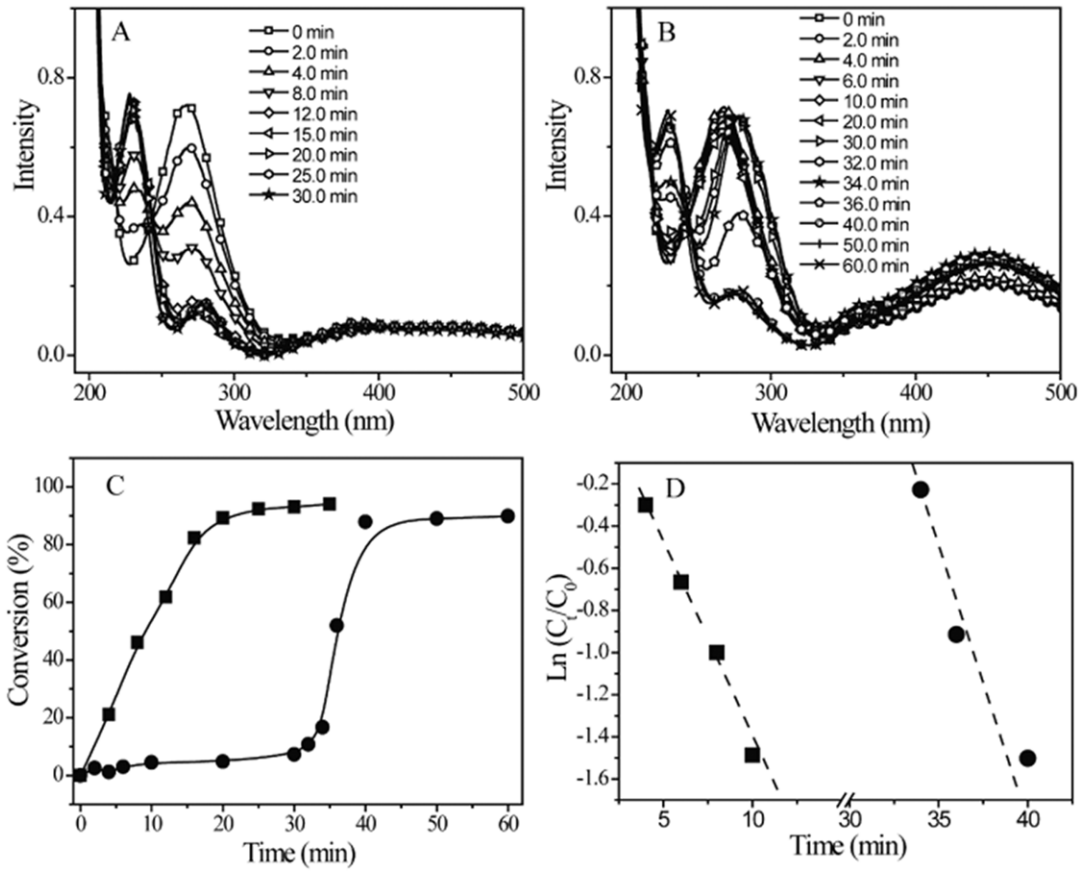

Figure 3. UV/vis spectra tracing the reduction of NB with Janus **3** prepared using 110.0 mmol l^{-1} ANI (A) and with Ag@PANI core–shell **4** possessing average PANI shell thicknesses 22 ± 5.0 (B). The conversion of NB (C) and the kinetics of the reduction of NB at low conversions (D) when using Ag–PANI Janus **3** catalyst (■) and core–shell **4** catalyst with shell thicknesses 22 ± 5.0 (●).

observed that the reduction of NB catalyzed by core–shell **1**–**5** with 2 ± 0.4, 5 ± 1.0, 11 ± 3.0, 22 ± 5.0 and 29 ± 7.0 nm of PANI shells had approximately 1.0, 2.0, 10.0, 30.0 and 50.0 min induction time, respectively (figure 4(A) and figure 9S available at stacks.iop.org/Nano/24/185602/mmedia). Since oxygen in the aqueous solutions was removed by purging them with argon for 30 min, it can be confirmed that the induction time was caused by the PANI shell, rather than the oxygen [26]. We also investigated the reaction kinetics of these reactions at relatively low conversions, when disregarding the induction period. Since the core–shell NPs with thicker PANI shells have a low content of Ag component, it is theoretically expected that the core–shell NPs with thicker PANI shells would exhibit lower catalytic capability if all the catalysts are used in the same concentration. However, the calculated K_{app} and K_1 unexpectedly show that core–shell NPs having thicker PANI shells exhibited higher catalytic capability (figure 4(B) and table 1). To further clarify the functionality of the PANI component on the catalytic property of the Janus and core–shell NPs, we comparatively investigated the catalytic capability of pure Ag NPs with average diameter 63.2 ± 5 nm in the reduction of NB (table 1 and figure 10S available at stacks.iop.org/Nano/24/185602/mmedia). Notably, the calculated K_{app} and K_1 of the Ag NPs were higher than Janus **3**, core–shell **1** and **2**, but lower than core–shell **3**–**5**. This result further confirmed that the PANI shell can facilitate the catalytic reaction.

We speculate that the PANI shell is the key factor that determines the duration time and the catalytic capability of the Ag@PANI core–shell NPs. Previous work has demonstrated that the PANI synthesized by using SDBS as surfactant exhibit significant hydrophobic properties [37]. It is possible for lipophilic NB to penetrate into the PANI shells (figure 4(C)). This means that the NB is absorbed and concentrated by the PANI shell during the induction period of the reaction (this can be confirmed by the evident red-shift and the intensity enhancement of the NB absorption peak in figure 3(B) and figure 9SD available at stacks.iop.org/Nano/24/185602/mmedia). Understandably, NB requires more time to penetrate through thicker PANI shells, thereby resulting in a longer induction period. Moreover, since a thicker PANI shell can concentrate more NB, it is reasonable to assume that the catalytic capability of the core–shell NPs increases with increasing PANI shell thickness. In the case of Ag–PANI Janus NPs, Ag NPs are exposed to the solution phase. NB tends to be directly catalyzed by Ag NPs, rather than penetrating into the PANI hemispheres (figure 4(D)). As a result, the PANI component in Janus NPs cannot concentrate the NB, therefore leading to a relatively lower catalytic capability (figure 3(D)).

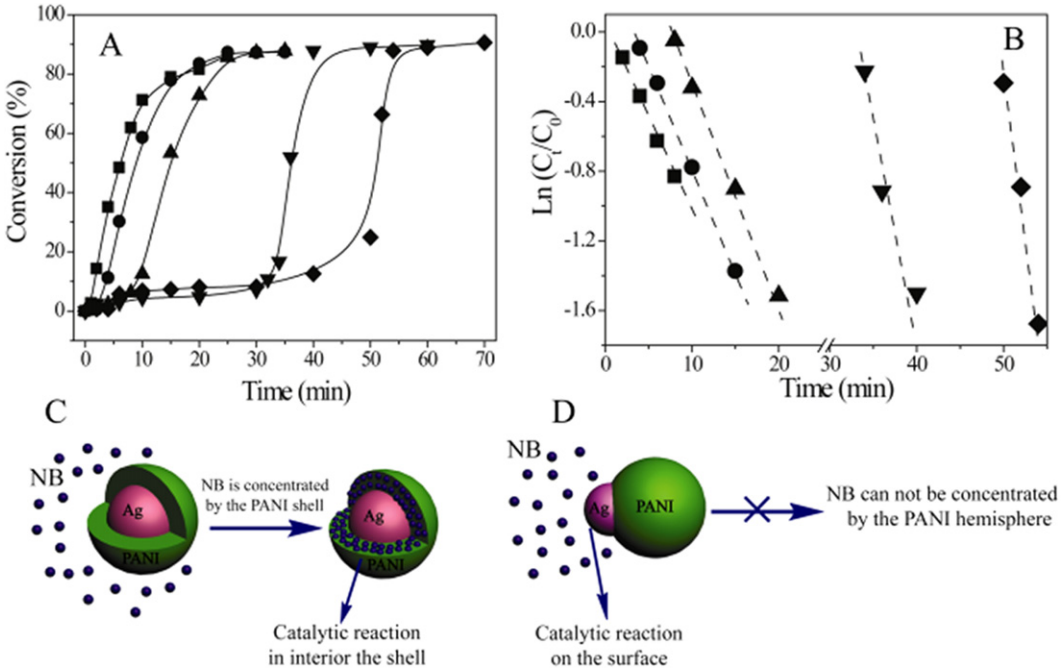

Figure 4. The conversion of NB (A) and the kinetics of the NB reduction at low conversions (B) when using core–shell **1**–**5** catalysts with different average PANI shell thicknesses (■) 2.0 ± 0.4, (●) 5.0 ± 1.0, (▲) 11.0 ± 3.0, (▼) 22 ± 5.0 and (♦) 29 ± 7.0 nm. (C) and (D) schematically show the reaction processes of the NB reduction catalyzed by core–shell NPs and Janus NPs, respectively.

Since the hydrophobic PANI shell can concentrate hydrophobic NB, and improve the catalytic capability of the encapsulated Ag NPs, we are also interested in testing whether this PANI shell can concentrate reagent with relatively higher hydrophilicity. 4-NP was chosen as a hydrophilic reagent for this experiment, because it possesses an evidently higher solubility in water than NB. In the catalytic reduction of 4-NP to 4-AP by using the Ag@PANI core–shell NP catalyst, we firstly added the Ag@PANI core–shell NPs, 4-NP and $NaBH_4$ solutions synchronously into a quartz cuvette filled with 2.0 ml deionized water. However, we did not observe any evident decrease of the characteristic absorption peak of 4-NP at 400 nm, or the emergence of the characteristic absorption peak of 4-AP at around 295 nm in the UV/vis spectra (figure 5(A) and its inset), which trace the reaction. This result clearly reveals that the Ag@PANI core–shell NPs have no catalytic capability in the reduction of 4-NP to 4-AP if the catalyst and the reactants participate in the reaction at the same time.

We then tried a special feeding sequence for this testing. 4-NP and Ag@PANI core–shell NPs aqueous solutions were first added into a quartz cuvette filled with 2.0 ml deionized water. After the mixture was left undisturbed for 0.5 h, $NaBH_4$ solution was added. Figures 5(B)–(D) give the UV/vis spectra running after the reduction of 4-NP with various Ag@PANI core–shell NP catalysts. Interestingly, it is clear that the characteristic absorption peak of 4-NP at 400 nm decreases gradually and the characteristic absorption peak of 4-AP at around 310 nm increases rapidly. This means that the Ag@PANI core–shell NPs have robust catalytic capability in the reduction of 4-NP when using this special feeding sequence. Figures 6(A) and (B) show the conversion and the reaction kinetics (under a relatively low conversion) as an function of PANI shell thickness. K_{app} (ranging from 8.0×10^{-4} to 9.3×10^{-4} s^{-1}) and K_1 (ranging from 3.57×10^{-2} to 6.59×10^{-2} s^{-1} m^{-2} l) calculated from these plots (table 1S) increase with increasing thickness of the PANI shell, revealing that a thicker PANI shell leads to a higher catalytic capability. This is almost the same as the trend of the catalytic capability when catalytically reducing the hydrophobic NB. Comparative investigation of the catalytic capability of Ag NPs in the reduction of 4-NP indicates that both K_{app} (5.90×10^{-4} s^{-1}) and K_1 (2.55×10^{-2} s^{-1} m^{-2} l) were lower than that of the core–shell NPs (figure 10S and table 1S available at stacks.iop.org/Nano/24/185602/mmedia). This result demonstrated that the PANI shell can also enhance the catalytic capability of the Ag@PANI core–shell NPs in the reduction of 4-NP.

Note that $NaBH_4$ was used in large excess during the catalytic reaction, NaOH derived from the oxidation of $NaBH_4$ can easily react with 4-NP to form nitrophenol sodium, which is completely water soluble. Consequently, it is understandable that the hydrophobic NB, rather than the hydrophilic nitrophenol sodium, can be absorbed and concentrated by the hydrophobic PANI shells (figures 4(C) and 6(C)). In other words, the hydrophobic PANI shells isolate Ag NPs from nitrophenol sodium, whereas they bridge Ag NPs with NB. We consider that this is the reason why Ag@PANI core–shell NPs show robust catalytic capability in the reduction of NB, but exhibit no catalytic capability in the reduction of 4-NP, when all the reactants participate in the reaction synchronously. However, when mixing Ag@PANI core–shell NPs and 4-NP in aqueous solution without $NaBH_4$, 4-NP can dope the PANI shells, as it is a type of weak acid.

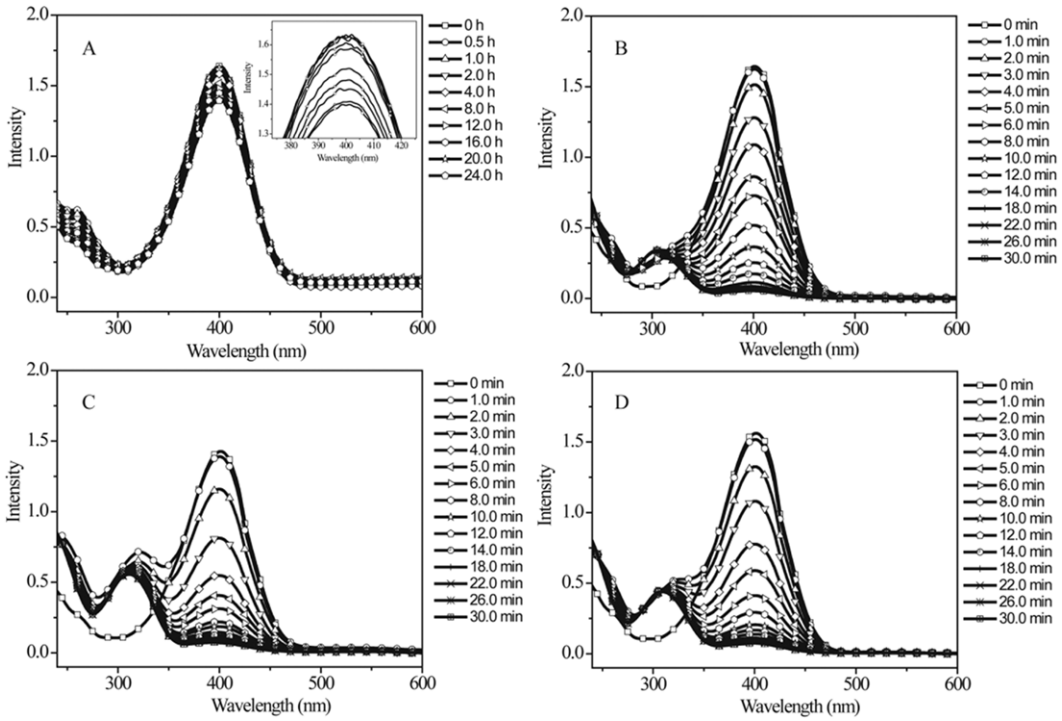

Figure 5. UV/vis spectra tracing the reduction of 4-NP with various Ag@PANI core–shell NPs. (A) Core–shell **1** with 2.0 ± 0.4 nm average shell thickness; during the experimental process, catalyst, 4-NP and $NaBH_4$ were added into the quartz cuvette synchronously. (B)–(D) Core–shell **1**, **3**, **5** with 2.0 ± 0.4, 11.0 ± 0.4 and 29.0 ± 7.0 nm average shell thicknesses, respectively; during the experimental process, catalyst and 4-NP were added into the quartz cuvette first, then $NaBH_4$ was added after 0.5 h. The inset of (A) is a magnified area of the spectra.

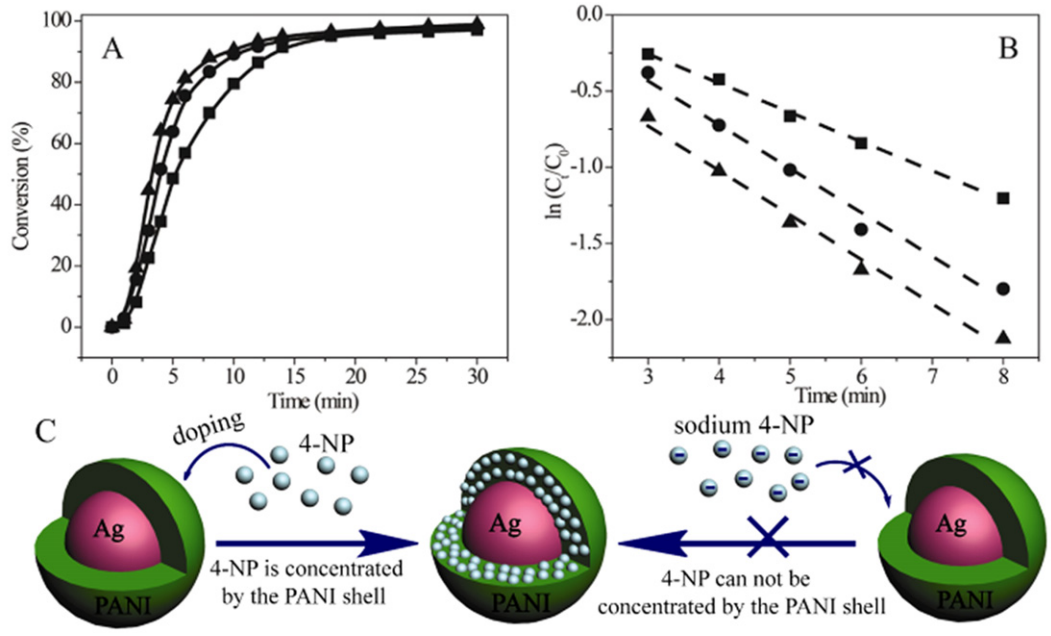

Figure 6. (A) The conversion of 4-NP using Ag@PANI core–shell NP catalysts with 2.0 ± 0.4 (■), 11.0 ± 3.0 (●) and 29.0 ± 7.0 nm (▲) average shell thicknesses. (B) Kinetics of the reduction of 4-NP fitted from the curves in (A) under low conversions. (C) Scheme illustrates the reaction processes of the 4-NP reduction catalyzed by core–shell NPs.

Driven by this, 4-NP molecules are absorbed and concentrated by the PANI shells (figure 6(C)). After the addition of $NaBH_4$, the catalytic reduction of 4-NP can take place smoothly because the absorbed 4-NP molecules have already been concentrated surrounding the Ag NPs. Moreover, we can further infer from this result that hydrophilic molecules, which can dope the PANI, will penetrate through the hydrophobic PANI shells and react with the encapsulated Ag NPs. As

the absorption of 4-NP is induced by the doping of PANI, it is easy to understand that Ag@PANI core–shell NPs with thicker PANI shells can absorb more 4-NP, which makes the catalytic reduction of 4-NP faster. Consequently, the catalytic capability of the Ag@PANI core–shell NPs increases with increasing PANI shell thickness (as shown in figures 6(A) and (B)). To this end, we suggest that the PANI shell is the key factor in the controllable catalytic capability and molecular recognition of the Ag@PANI core–shell NPs.

4. Conclusions

In summary, on the basis of a facile hydrothermal route, we have selectively constructed Ag–PANI Janus NPs and Ag@PANI core–shell NPs at hydrothermal temperatures 105 and 125 °C, respectively. While the morphology of the hybrid nanocomposites was determined by hydrothermal temperature, we also found that the diameters of Janus NPs and the PANI shell thickness of core–shell NPs could be controlled via a simple adjustment of the ANI concentration. Coating the Ag NPs with hydrophobic PANI shells is of particular interest, since the PANI shells can concentrate the hydrophobic reagent, thus improving the catalytic capability of the core–shell NPs. In the catalytic property evaluation of the composite nanostructures, we have found that: (i) Ag@PANI core–shell NPs exhibit an unexpectedly higher catalytic capability than Ag–PANI Janus NPs in the reduction of hydrophobic NB; (ii) core–shell NPs with thicker PANI shells have relatively higher catalytic capability when catalytically reducing NB; (iii) tuning the property (undoping/doping state) of the PANI shell can easily switch the catalytic reduction of hydrophilic 4-NP. We believe that the proposed hydrothermal route may prove to be a simple and effective synthetic method to construct noble metal–polymer nanocomposites with well-defined morphologies. More importantly, this work also opens an avenue to the improvement and control of catalytic capabilities in the field of catalysis, especially in aqueous medium catalysis.

Acknowledgments

This work was supported by the National Natural Science Foundation of China (51173153, U1205113); the Special Program for Key Research of Chinese National Basic Research Program (2011CB612303) and Xiamen Science and Technology Committee (No. 3502Z20121021, 3502Z20120015).

References

[1] Teranishi T, Inoue Y, Nakaya M, Oumi Y and Sano T 2004 *J. Am. Chem. Soc.* **126** 9914
[2] Yu H, Chen M, Rice P M, Wang S X, White R L and Sun S 2005 *Nano Lett.* **5** 379
[3] Ge J, Hu Y, Zhang T and Yin Y 2007 *J. Am. Chem. Soc.* **129** 8974
[4] Reculusa S, Poncet-Legrand C, Ravaine S, Mingotaud C, Duguet E and Bourgeat-Lami E 2002 *Chem. Mater.* **14** 2354
[5] Wang B, Li B, Zhao B and Li C Y 2008 *J. Am. Chem. Soc.* **130** 11594
[6] Xing S, Feng Y, Tay Y Y, Chen T, Xu J, Pan M, He J, Hng H H, Yan Q and Chen H 2010 *J. Am. Chem. Soc.* **132** 9537
[7] Kietzke T, Neher D, Landfester K, Montenegro R, Güntner R and Scherf U 2003 *Nature Mater.* **2** 408
[8] Higuchi T, Tjima A, Motoyoshi K, Yabu H and Shimomura M 2008 *Angew. Chem.* **120** 8164
[9] Wurm F, König H M, Hilf S and Kilbinger A F M 2008 *J. Am. Chem. Soc.* **130** 5876
[10] Paunov V N 2003 *Langmuir* **19** 7970
[11] Paunov V N and Cayre O J 2004 *Adv. Mater.* **16** 788
[12] Cayre O, Paunov V N and Velev O D 2003 *J. Mater. Chem.* **13** 2445
[13] Jiang S and Granick S 2008 *Langmuir* **24** 2438
[14] Fujimoto K, Nakahama K, Shidara M and Kawaguchi H 1999 *Langmuir* **15** 4630
[15] Nakahama K, Kawaguchi H and Fujimoto K 2000 *Langmuir* **16** 7882
[16] Nisisako T, Torii T, Takahashi T and Takizawa Y 2006 *Adv. Mater.* **18** 1152
[17] Kim S H, Jeon S J, Jeong W C, Park H S and Yang S M 2008 *Adv. Mater.* **20** 4129
[18] Gorelikov I, Field L M and Kumacheva E 2004 *J. Am. Chem. Soc.* **126** 15938
[19] Nayak S and Lyon L A 2005 *Angew. Chem. Int. Edn* **44** 7686
[20] Kang Y and Taton T A 2005 *Angew. Chem. Int. Edn* **44** 409
[21] Álvarez-Puebla R, Contreras-Cáceres R, Pastoriza-Santos I, Pérez-Juste J and Liz-Marzán L M 2009 *Angew. Chem. Int. Edn* **48** 138
[22] Contreras-Cáceres R, Pacifico J, Pastoriza-Santos I, Pérez-Juste J, Fernández-Barbero A and Liz-Marzán L M 2009 *Adv. Funct. Mater.* **19** 3070
[23] Contreras-Cáceres R, Sánchez-Iglesias A, Karg M, Pastoriza-Santos I, Pérez-Juste J, Pacifico J, Hellweg T, Fernández-Barbero A and Liz-Marzán L M 2008 *Adv. Mater.* **20** 1666
[24] Zhang X and Su Z 2012 *Adv. Mater.* **24** 4574
[25] Lu Y, Mei Y, Drechsler M and Ballauff M 2006 *Angew. Chem. Int. Edn* **45** 813
[26] Mei Y, Lu Y, Polzer F and Ballauff M 2007 *Chem. Mater.* **19** 1062
[27] Schrinner M, Proch S, Mei Y, Kempe R, Miyajima N and Ballauff M 2008 *Adv. Mater.* **20** 1928
[28] Lu Y, Mei Y and Ballauff M 2006 *J. Phys. Chem.* B **110** 3930
[29] Fang X, Ma H, Xiao S, Shen M, Guo R, Cao X and Shi X 2011 *J. Mater. Chem.* **21** 4493
[30] Oliveira M M, Castro E G, Canestraro C D, Zanchet D, Ugarte D, Roman L S and Zarbin A J G 2006 *J. Phys. Chem.* B **110** 17063
[31] Karim M R, Lim K T, Lee C J, Bhuiyan M T L, Kim H J, Park L-S and Lee M S 2007 *J. Polym. Sci.* A **45** 5741
[32] Helms B, Liang C O, Hawker C J and Fréchet J M J 2005 *Macromolecules* **38** 5411
[33] Ge Z, Xie D, Chen D, Jiang X, Zhang Y, Liu H and Liu S 2007 *Macromolecules* **40** 3538
[34] O'Reilly R K, Hawker C J and Wooley K L 2006 *Chem. Soc. Rev.* **35** 1068
[35] Lu A, Moatsou D, Longbottom D A and O'Reilly R K 2013 *Chem. Sci.* **4** 965
[36] Yuan C, Luo W, Zhong L, Deng H, Liu J, Xu Y and Dai L 2011 *Angew. Chem. Int. Edn* **50** 3515
[37] Isaksson J, Tengstedt C, Fahlman M, Robinson N and Berggren M 2004 *Adv. Mater.* **16** 316